2013

Enhancing mechanical properties of a low-carbon microalloyed cast steel by controlled heat treatment

Jingwei Zhao
University of Wollongong, jzhao@uow.edu.au

Jeong Hun Lee
Pohang University of Science and Technology

Yong Woo Kim
Pohang University of Science and Technology

Zhengyi Jiang
University of Wollongong, jiang@uow.edu.au

Chong Soo Lee
Pohang University of Science and Technology

Publication Details

Zhao, J., Hun Lee, J., Kim, Y. Woo., Jiang, Z. & Lee, C. Soo. (2013). Enhancing mechanical properties of a low-carbon microalloyed cast steel by controlled heat treatment. Materials Science and Engineering A: Structural Materials: Properties, Microstructure and Processing, 559 427-435.

Enhancing mechanical properties of a low-carbon microalloyed cast steel by controlled heat treatment

Abstract
In the present work, detailed studies were made on the optimization of microstructure and mechanical properties of a low-carbon microalloyed cast steel through control of heat treatment conditions. Specimens were austenitized at temperatures ranging from 950 to 1200 °C for 2 h followed by different cooling methods (furnace, air and water). For analyzing the effect of holding time on mechanical properties, some cast specimens were austenitized at 1100 °C for different times followed by furnace cooling. After heat treatment, mechanical tests were employed to evaluate the room temperature Charpy impact and tensile properties. The characterization of complex precipitates formed during heat treatment process was investigated by using analytical electron microscopy. The results show that dissolution of vanadium-containing precipitates plays an important role in the abnormal growth of austenite grains at 1150 °C. Further growth in austenite grains at 1200 °C is caused by the dissolution of Ti-containing particles and the reduction of the amount of precipitates. Correct selection of the austenitizing temperature, holding time and cooling method is very important to improve the mechanical properties of the steel. Heat treatment at 1100 °C for 2 h followed by furnace cooling leads to the best combination of excellent Charpy impact and tensile properties.

Keywords
mechanical, enhancing, heat, treatment, controlled, steel, cast, microalloyed, carbon, low, properties

Disciplines
Engineering | Science and Technology Studies

Publication Details
Zhao, J., Hun Lee, J., Kim, Y. Woo., Jiang, Z. & Lee, C. Soo. (2013). Enhancing mechanical properties of a low-carbon microalloyed cast steel by controlled heat treatment. Materials Science and Engineering A: Structural Materials: Properties, Microstructure and Processing, 559 427-435.

Enhancing mechanical properties of a low-carbon microalloyed cast steel by controlled heat treatment

Jingwei Zhao[1,2], Jeong Hun Lee[1], Yong Woo Kim[1], Zhengyi Jiang[2], Chong Soo Lee[1,3,*]

[1]Department of Materials Science and Engineering, Pohang University of Science and Technology, Pohang 790-784, Korea

[2]School of Mechanical, Materials and Mechatronic Engineering, University of Wollongong, NSW 2522, Australia

[3]Graduate Institute of Ferrous Technology, Pohang University of Science and Technology, Pohang 790-784, Korea

Abstract

In the present work, detailed studies were made on the optimization of microstructure and mechanical properties of a low-carbon microalloyed cast steel through control of heat treatment conditions. Specimens were austenitized at temperatures ranging from 950 to 1200 ℃ for 2 h followed by different cooling methods (furnace, air and water). For analyzing the effect of holding time on mechanical properties, some cast specimens were austenitized at 1100 ℃ for different times followed by furnace cooling. After heat treatment, mechanical tests were employed to evaluate the room temperature Charpy impact and tensile properties. The characterization of complex precipitates formed during heat treatment process was investigated by using analytical electron microscopy. The results show that dissolution of vanadium-containing precipitates plays an important role in the abnormal growth of austenite grains at 1150 ℃. Further growth in austenite grains at 1200 ℃ is caused by the dissolution of Ti-containing particles and the reduction of the amount of precipitates. Correct selection of the austenitizing temperature, holding time and cooling method is very important to improve the mechanical properties of the steel. Heat treatment at 1100 ℃ for 2 h followed by furnace cooling leads to the best combination of excellent Charpy impact and tensile properties.

Keywords: Microalloyed cast steel; Heat treatment; Toughness; Strength; Precipitates

* Corresponding author. Tel.: +82-54-279-2141; Fax: +82-54-279-2399.

E-mail addresses: jwzhaocn@gmail.com (J. Zhao), cslee@postech.ac.kr (C.S. Lee).

1. Introduction

Low-carbon steels, steels with carbon content less than 0.25%, make up the highest tonnage of all steels produced in a given year. Research on low-carbon structural steels has been very active during the past several years because of the emphasis placed on the extensive application in the field of structures, automotive components, bridges and buildings [1-4]. To improve load bearing, recent approaches have been focused on developing low-carbon microalloyed steels with excellent combinations of fracture resistance and strength for given applications in order to reduce section size and weight. The addition of alloying elements, such as titanium (Ti), niobium (Nb) and vanadium (V), offers an important cost-effective approach to obtain a good combination of excellent toughness and strength through grain size control and precipitation hardening [5].

In order to achieve the desired mechanical properties, hot deformation approaches including forging and hot rolling are generally used in low-carbon microalloyed cast steels [6,7]. Even though hot deformation is an effective method to improve the toughness and strength, the production procedure, energy consumption and then production cost will certainly be increased. If direct processing method, such as the heat treatment, after casting is available to improve both toughness and strength to an acceptable level, the problem above can be solved, and the production cost will be undoubtedly reduced. Consequently, demands for producing low-cost, higher strength steels castings with excellent toughness and strength have encouraged many researchers to focus on microalloyed cast steels. Nowadays, microalloyed cast steels have found many applications in the manufacturing of industrial parts such as offshore platform nodes, machinery supports, natural gas compressor housing, ingot moulds and buckets [8]. Since most of these parts have to be heat treated before use, many efforts were made on the effects of different heat treatment variables on the microstructure and mechanical properties of microalloyed cast steels. Voigt and Rassizadehghani [9] studied the influence of heat treatment and chemical composition on the properties of microalloyed cast steels, and they found that the yield strength levels up to 690 MPa could be achieved after quench and temper heat treatments combined with good toughness. The work of Jana et al. [10] indicated that the tensile strength and elongation of microalloyed cast steels were significantly increased via controlled heat treatment.

In low-carbon microalloyed steels, the austenite grain growth behavior is closely related to the precipitates. Fine precipitate dispersions of the microalloying elements retard austenite growth, and the more stable the precipitates,

the more effectively grain growth is retarded to higher temperatures [11]. Previous research has studied the dissolution behavior of precipitates at typical reheating temperatures. Balasubramanian et al. [12] carried out an investigation on the solubility of titanium carbide in the temperature range of 1273 to 1473 K using a dynamic gas equilibrium technique. Inoue et al. [13] found that the immiscibility of carbonitride strongly affected the phase equilibria even when the content of microalloying elements in steels was very low. The research was mainly based on the thermodynamic stability of the precipitating phases. Since the solubility products do not take into consideration of the effect of co-precipitation (complex precipitates formed with two or more microalloying elements present), significant variation in the dissolution temperatures predicted by solubility products is usually caused. Accordingly, the dissolution behavior of complex precipitates at various reheating temperatures cannot be accurately predicted by using these methods.

This study aims to enhance both the toughness and strength of a low-carbon microalloyed cast steel to an appreciate level through application of heat treatment with discussion on the mechanisms of enhancement of mechanical properties. Dissolution behaviors of complex precipitates at various heat treatment temperatures are investigated, and the relationship between the austenite grain growth and precipitate dissolution is analyzed.

2. Experimental procedure

The material used in this study is a low-carbon microalloyed cast steel. The chemical compositions in weight percentage are reported in Table 1.

Fig. 1 shows the metallograph of the as-cast steel. As demonstrated, dendrite microstructure was caused during casting process. The following examinations and tests were carried out on the material.

2.1. Heat treatment

Prior to heat treatment, two groups of rectangular specimens with size of 12 mm × 12 mm × 60 mm and 12 mm × 12 mm × 110 mm respectively were cut from the cast steel. Heat treatment was carried out using an electric furnace in laboratory. Some of the specimens were initially austenitized at temperatures ranging from 950 to 1200 ℃ in steps of 50 ℃for 2 h and then were cooled in different mediums (furnace, air and water). In order to determine the optimum

austenitizing time, some of the specimens were austenitized at 1100 ℃ for 0.5 and 5 h respectively followed by furnace cooling.

2.2. Mechanical properties tests

After heat treatment, standard Charpy impact and tensile specimens were machined according to ASTM E 23 and ASTM E 8M, respectively. The Charpy V-notched specimens with cross section of 10 mm × 10 mm, length of 55 mm, notch angle of 45° and notch depth of 2 mm were employed to study the room temperature (RT) impact resistance on a Zwick/Roell impact tester. Tensile tests were performed using standard specimens (Gauge length 30 mm, gauge diameter 6 mm) on an INSTRON 8801 tensile testing machine at RT with strain rate of 5×10^{-3} s^{-1}. The yield strength (YS, 0.2% proof stress), ultimate tensile strength (UTS) and percent elongation were directly recorded from the results displayed by computer on the monitor.

2.3. Metallography and fractography

Optical microscopy (OM), scanning electron microscopy (SEM) and transmission electron microscope (TEM) were used to identify microstructures. For OM observation, specimens were metallographically polished and then etched in a solution mixed with picric acid and absolute alcohol. Element segregation analysis of the as-cast steel was carried out using energy dispersive X-ray spectroscopy (EDS) on SEM at an accelerating voltage of 15 kV.

In low-carbon steels where equiaxed ferrite grains grow across austenite grain boundaries and make up most of the microstructure, delineation of austenite boundaries by ferrite is not effective. Quenching from austenite phase field to produce martensite that marks the extent of austenite grains has been effectively used to measure the grain size in low-carbon steels [14]. In the present work, therefore, the water quenched specimens were etched with a “picric acid + $FeCl_3$ + dodecyl benzene sulfonic acid sodium salt” solution to reveal prior austenite grain boundaries, and then observed by SEM.

For examining the character and composition of the precipitates during heat treatment, extraction replicas as well as thin foils mounted on Cu grids of water quenched specimens were prepared and analyzed using EDS method on

TEM operated at 200 kV. Fracture surfaces of the tested specimens were examined on SEM using an accelerating voltage of 15 kV to determine the failure mode.

3. Experimental results

3.1. Mechanical properties

3.1.1. Charpy impact properties

The RT impact energies of both as-cast and heat-treated specimens are given in Table 2. It can be seen that the specimen austenitized at 1100 ℃ for 2 h followed by furnace cooling shows the highest impact energy of 120.3 J, which is about 22 times higher than that of as-cast one. Fig. 2 shows the dependence of RT impact energy on heat treatment temperature of the specimens after 2 h austenitization. It is clear that the impact energy of the specimen cooled in furnace is higher than those cooled in air and water at a fixed temperature. Moreover, the impact energy of the furnace-cooled specimen increases gradually at first, then to a maximum value at the temperature of 1100 ℃, and finally it drops dramatically when the temperature is higher than 1100 ℃.

3.1.2. Tensile properties

RT tensile tests were performed on the furnace-cooled specimens, and the typical tensile curves are shown in Fig. 3. The tensile properties obtained from Fig. 3 are presented in Table 3. The results in Fig. 3 indicate that the tensile behaviors of the tested specimens are similar. Based on the results shown in Table 3, the specimen austenitized at 950 ℃ for 2 h and cooled in furnace (HT1F) shows the highest YS (378.5 MPa) and UTS (541.6 MPa) with elongation of 29.4%, while the specimen austenitized at 1100 ℃ for 2 h and cooled in furnace (HT4F) shows the highest value of elongation (34.3%) with YS and UTS of 344.9 and 511.3 MPa, respectively. However, taking the impact properties into consideration, the specimen HT4F shows higher impact resistance than that of specimen HT1F. To evaluate the mechanical properties, other measurements, such as the microstructure and fracture surface, are therefore necessary to be carried out on the specimens.

3.2. Microstructures

The OM microstructures of furnace-cooled specimens according to Table 2 are presented in Fig. 4. It can be seen that the microstructures consist of equiaxed ferrite and pearlite. Austenitizing temperature has a significant effect on the distribution of pearlite. When the temperature is low, the pearlite shows ring-shaped distribution features (Fig. 4a). With an increase of temperature, the ring-shaped pearlite cluster tends to be broken up into separate ones, and the pearlite distribution becomes more and more uniform, as shown in Fig. 4b, c and d. Although the heat treatment at temperatures 1150 and 1200 ℃ homogenized the microstructures (Fig. 4e and f), the negative effect on grain growth is clear compared to the specimens heat treated at lower temperatures. The effect of holding time on the pearlite distribution is clearly seen in Fig. 4d, g and h. Obviously, short holding time is not effective in homogenizing the microstructure (Fig. 4g). If the holding time is long (5 h in the present study), some of the grains grow abnormally (Fig. 4h).

The OM microstructures of specimens austenitized at 1100 ℃ for 2 h followed by air cooling and water quenching are shown in Fig. 5a and b, respectively. As shown in Fig. 5a, the microstructure of air-cooled specimen is mainly composed of polygonal ferrite and pearlite, accompanied with small quantity of Widmanstätten ferrite (WF). WF has a coarse, elongated morphology, readily resolved in the light microscope. WF forms at faster cooling rates than polygonal ferrite and in temperature ranges just below those at which equiaxed ferrite forms [15]. The microstructure of the water quenched specimen consists of full martensite, as shown in Fig. 5b.

Fig. 6a and b show the variation of ferrite grain size with temperature and holding time, respectively. As demonstrated in Fig. 6a, the ferrite grain size increases slightly with temperature in the temperature range of 950 to 1100 ℃, then suddenly increase in ferrite grain size when the temperature is higher than 1100 ℃. According to the result of Fig. 6b, the effect of holding time on ferrite grain size is insignificant. With regard to Figs. 4 and 6, the specimen HT4F shows the best combination of uniformly distributed microstructure and fine ferrite grains.

3.3. Fractography

Selected fracture surfaces in the shear lip areas of some impact test specimens are demonstrated in Fig. 7. As can be seen in Fig. 7a, the fracture surface of specimen HT0 is composed of large cleavage facets and shear cracks, which indicates the brittle nature of fracture. The fracture mode has been remarkably changed after heat treatment. The

fracture surface of specimen HT1F is a mixture of large dimples and small cleavage facets, as shown in Fig. 7b. Small, deep and uniformly distributed dimples are observed in the fracture surface image of specimen HT4F, which shows a characteristic of ductile fracture (Fig. 7c). However, as shown in Fig. 7d, the fracture mode of the specimen austenitized at 1150 ℃ for 2 h and cooled in furnace (HT5F) becomes cleavage-type again. According to these results, a critical temperature is necessary for obtaining ductile mode fracture. Moreover, neither shorter nor longer holding time are favorable to generate small, deep and uniformly distributed dimples after impact tests (Fig. 7e and f).

According to the above results, when the temperature is lower than 1100 ℃, the uniform distribution of pearlite significantly affects the impact energy. Slight increase in ferrite grain size with temperature shows inconspicuous effect on the impact energy. Sharp decrease of impact energy is caused by the rapid growth of ferrite grains as the temperature is elevated to 1150 ℃. Intact and small-sized ring of pearlite distributed at 950 ℃ is of advantage to increase the tensile strength. In the temperature range of 950 to 1100 ℃, the more uniform the pearlite distribution, the higher elongation is. Moreover, coarsening of ferrite grain size has a negative effect on the enhancement of elongation. Taking into account the impact energy, tensile strength, elongation, microstructure and fracture morphology, the specimen HT4F exhibits the best combination of excellent mechanical properties and optimal microstructure. Compared with the European Standard [16], the mechanical properties of HT4F show a good fit to the requirement of S275 and S355 steels. Even though for S420 steels, the required mechanical properties can also be satisfied in the large nominal thickness range.

4. Analysis and discussion

4.1. Microstructural distribution

Considerable diffusion of carbon is necessary for austenite formation to balance the carbon in various phases of the reaction. Cementite is the source of carbon for the austenite nucleation, and therefore the reaction begins at carbon rich ferrite/cementite interfaces. After nucleation, the further growth is still dependent on carbon diffusion through the surrounding austenite to austenite/ferrite interfaces. So, the distribution and diffusion of carbon have an important effect on the austenite formation and growth.

Fig. 8 shows the result of EDS line-scanning across a dendrite boundary, where high carbon peak is found, for the

as-cast specimen. According to this result, severe carbon segregation was caused during solidification, leading to non-uniform distribution of carbon in the as-cast specimen. When the as-cast specimen was heated to the austenitizing temperature, austenite formed accompanied with carbon diffusion in the matrix. Because the diffusion is strongly influenced by temperature [17], limited carbon diffusion occurs if the austenitizing temperature is low, and non-uniform distributed austenite is then considered to be formed. Fig. 9 shows the prior austenite grains of the water-quenched specimen after holding at 950 ℃ for 2 h. It can be seen that the distribution of prior austenite grains is non-uniform. Coarse grains, around which lots of fine grains are observed, distribute discontinuously in the matrix.

Pearlite is composed of alternate layers of cementite and ferrite. For slowly cooled low-carbon steel, the proeutectoid ferrite reaction precedes the pearlite reaction. Pearlite forms from austenite by a nucleation and growth process. It is generally accepted that pearlite nucleates preferentially at austenite grain boundaries [18]. For an austenite structure with uniform composition and grains, the free energy available for the formation of nuclei is the same in every volume element. Accordingly, the nucleation probability of pearlite is same at different austenite grain boundaries, and uniform distributed ferrite-pearlite microstructure will be obtained. In the case of non-uniform distribution of austenite grains, fine austenite grains supply greater available number of nucleation sites and higher activation energy for nucleation compared to that of coarse grains. For reducing free energy, the boundaries of fine austenite grains will be the preferred sites for pearlite nucleation. Moreover, the austenite/pearlite transformation rate increases with a decrease of austenite grain size due to an increase in nucleation rate of pearlite [19]. In other words, the regions with fine grains preferentially nucleate when austenite/pearlite phase transformation occurs. Finally, as schematically represented in Fig. 9 with dark circle (fine austenite grains run around the coarse ones), ring-shaped distribution characteristic of pearlite will be displayed after austenite/pearlite phase transformation (Fig. 4a). With the increase of austenitizing temperature and holding time, austenite distribution becomes more and more uniform, and subsequently, uniformly distributed pearlite will be available. The higher the austenitizing temperature and the longer the holding time, the more uniform the pearlite distribution will be, as shown in Fig. 4.

4.2. Grain growth

Many characteristics in steel, such as mechanical properties and the microstructures of austenite transformation products, depend on the austenite grain size. In low-carbon steel, the austenite grain size has a critical effect on the

formation of fine-grain ferritic microstructure with high toughness and strength. Fig. 10a and b show the dependence of prior austenite grain size on austenitizing temperature and holding time, respectively. As can be seen, the austenite grain size slightly increases as the temperature increases from 950 to 1100 ℃. When the temperature is higher than 1100 ℃, sharp increase in austenite grain size is observed. Moreover, holding time shows little influence on the austenite grain size. According to Figs. 6 and 10, it is clear that the ferrite grain size shows the same variable tendency with that of austenite grain size.

4.3. Characterization of complex precipitates

Figs. 11 - 14 show the character and composition of precipitates in the specimens austenitized at 950, 1100, 1150 and 1200 ℃ for 2 h followed by water quenching, respectively. When austenitized at 950 ℃, large numbers of precipitates are found, and the precipitates can be classified into two types in shape, i.e. irregular shape and rectangle (Fig. 11a). Additional EDS analysis shows that both irregularly shaped (Fig. 11b) and rectangular (Fig. 11c) particles contain Ti, Nb and V elements. Based on the compositions given in Table 1 and prior work [20,21], the precipitates are probably Ti, Nb and V carbides, nitrides or carbonitrides. Moreover, both spectra show high Cu, Si and O peaks. The Cu peaks are from the Cu grid. The Si and O peaks may correspond to silica or silicic acid formed by oxidation and hydration of the Si in the steel during the electrochemical extraction [22]. At 1100 ℃, square and rectangle are found to be the two types of precipitates (Fig. 12a). The square particle contains Ti, Nb and V, while only Ti and Nb are found in rectangular particles, as seen in Fig. 12b and c. When the austenitizing temperature is elevated to 1150 and 1200 ℃, just rectangular precipitates, which only contain Ti and Nb, exist in the matrix, as shown in Figs. 13 and 14.

Table 4 shows the results of composition analysis of precipitates obtained from spectra. As can be seen, increasing temperature from 950 to 1150 ℃ leads to remarkable decrease in the content of Nb and V in precipitates. Further increasing temperature to 1200 ℃ causes leaner Ti content in the precipitate compared with that at 1150 ℃. Since titanium nitride TiN is the most stable and is known to have a dissolution temperature above the iron liquidus temperature, it is probable that TiN is the initial precipitate, and Nb or V mostly forms on the outside layer of TiN to be the complex precipitate. In fact, because Ti, Nb and V carbides, nitrides or carbonitrides have similar crystal structures, co-precipitation is very common in multi-microalloyed steels [20]. Based on Fig. 10 and Table 4, it can be deduced that the dissolution of Nb- and V-containing precipitates has no significant effect on the austenite grains

growth when the temperature is lower than 1100 ℃. However, the dissolution of V-containing precipitates plays a key role in the abnormal growth of austenite grains when the temperature increases from 1100 to 1150 ℃. When the austenitizing temperature is increased to 1200 ℃, significant reduction of the amount of precipitates will be caused [23]. Therefore, further growth in austenite grains at 1200 ℃ should be attributed to the dissolution of Ti-containing particles and the reduction of the amount of precipitates.

5. Conclusions

An investigation has been made on the optimization of microstructure and mechanical properties of a low-carbon microalloyed cast steel through control of heat treatment conditions. The characterization of complex precipitates formed during heat treatment process was investigated by using analytical electron microscopy. The following conclusions are drawn from the present work:

1. Correct selection of the austenitizing temperature, holding time and cooling method is very important to improve the mechanical properties. Heat treatment at 1100 ℃ for 2 h followed by furnace cooling results in the best combination of excellent impact and tensile properties. The combinations in the present steel are: Charpy impact energy: 120.3 J, YS: 344.9 MPa, UTS: 511.3 MPa and elongation: 34.3%.

2. Carbon segregation affects significantly on the distribution uniformity of austenite during heat treatment. As austenitizing temperature and holding time increase, austenite distribution becomes more and more uniform, and subsequently uniformly distributed pearlite is obtained.

3. The morphology and composition of complex precipitates vary with austenitizing temperatures. Dissolution of V-containing precipitates plays an important role in the abnormal growth of austenite grains at 1150 ℃. Further growth in austenite grains at 1200 ℃ is caused by the dissolution of Ti-containing particles and the reduction of the amount of precipitates.

References

[1] M.A. Bepari, J.A. Whiteman, J. Mater. Process. Technol. 56 (1996) 834-846.

[2] R. Mendoza, J. Huante, M. Alanis, C. Gonzalez-Rivera, J.A. Juarez-Islas, Mater. Sci. Eng. A 276 (2000) 203-209.

[3] J. Guo, C. Shang, S. Yang, H. Guo, X. Wang, X. He, Mater. Des. 30 (2009) 129-134.

[4] A. Avci, N. Ilkaya, M. Simsir, A. Akdemir, J. Mater. Process. Technol. 209 (2009) 1410-1416.

[5] B.K. Show, R. Veerababu, R. Balamuralikrishnan, G. Malakondaiah, Mater. Sci. Eng. A 527 (2010) 1595-1604.

[6] M. Jahazi, B. Eghbali, J. Mater. Process. Technol. 113 (2001) 594-598.

[7] S.K. Das, S. Chatterjee, S. Tarafder, J. Mater. Sci. 44 (2009) 1094-1100.

[8] H. Najafi, J. Rassizadehghani, S. Asgari, Mater. Sci. Eng. A 486 (2008) 1-7.

[9] R.C. Voigt, J. Rassizadehghani, AFS Trans. 103 (1995) 791-802.

[10] B.D. Jana, A.K. Chakrabarti, K.K. Ray, Mater. Sci. Technol. 19 (2003) 80-86.

[11] O. Flores, L. Martinez, J. Mater. Sci. 32 (1997) 5985-5991.

[12] K. Balasubramanian, A. Kroupa, J.S. Kirkaldy, Metall. Trans. A 23 (1992) 709-727.

[13] K. Inoue, N. Ishikawa, I. Ohnuma, H. Ohtani, K. Ishida, ISIJ Int. 41 (2001) 175-182.

[14] S.S. Hansen, J.B. Vander Sande, M. Cohen, Metall. Trans. A 11 (1980) 387-402.

[15] G. Krauss, Steels: Processing, Structure, and Performance, ASM International, Ohio, 2005, pp. 109-111.

[16] EN 10025-3, Hot rolled products of structural steels-Part 3: Technical delivery conditions for normalized/normalized rolled weldable fine grain structure steels, British Standards Institution, London, 2004, pp. 17-21.

[17] J. Kučera, K. Stránský, Mater. Sci. Eng. 52 (1982) 1-38.

[18] S.A. Hackney, G.J. Shiflet, Acta Metall. 35 (1987) 1019-1028.

[19] S. Serajzadeh, A.K. Taheri, Mater. Des. 25 (2004) 673-679.

[20] R.M. Poths, R.L. Higginson, E.J. Palmiere, Scr. Mater. 44 (2001) 147-151.

[21] H.R. Wang, W. Wang, J. Mater. Sci. 44 (2009) 591-600.

[22] R.W. Gurry, J. Christakos, C.D. Stricker, Trans. ASM 50 (1958) 105-128.

[23] R.D. Fu, T.S. Wang, W.H. Zhou, W.H. Zhang, F.C. Zhang, Mater. Charact. 58 (2007) 968-973.

Figure Captions:

Fig. 1. Metallograph of the as-cast steel.

Fig. 2. Plots of RT impact energy vs. heat treatment temperature at various cooling conditions after 2 h austenitization.

Fig. 3. Typical tensile curves of the furnace-cooled specimens.

Fig. 4. OM microstructures of furnace-cooled specimens according to Table 2: (a) HT1F, (b) HT2F, (c) HT3F, (d) HT4F, (e) HT5F, (f) HT6F, (g) HT4F1, and (h) HT4F2.

Fig. 5. OM microstructures of selected specimens according to Table 2: (a) HT4A, and (b) HT4W (etched by nital).

Fig. 6. Effect of temperature and holding time on ferrite grain size of the heat treated specimens after furnace cooling with (a) holding time of 2 h and (b) austenitizing temperature of 1100 ℃.

Fig. 7. Selected fracture surfaces in the shear lip areas of some impact test specimens according to Table 2: (a) HT0, (b) HT1F, (c) HT4F, (d) HT5F, (e) HT4F1, and (f) HT4F2.

Fig. 8. Line-scanning for the as-cast specimen shows C segregation along dendrite boundary.

Fig. 9. SEM image of specimen HT1W shows non-uniform distribution of prior austenite grains.

Fig. 10. Effect of temperature and holding time on the prior austenite grain size of the heat treated specimens after water quenching with (a) holding time of 2 h and (b) austenitizing temperature of 1100 ℃.

Fig. 11. Character and composition of precipitates in the specimen austenitized at 950 ℃: (a) Dark field image, (b) EDS of particle “b”, and (c) EDS of particle “c”.

Fig. 12. Character and composition of precipitates in the specimen austenitized at 1100 ℃: (a) Dark field image, (b) EDS of particle “b”, and (c) EDS of particle “c”.

Fig. 13. Character and composition of precipitates in the specimen austenitized at 1150 ℃: (a) Dark field image, and (b) EDS of particle.

Fig. 14. Character and composition of precipitates in the specimen austenitized at 1200 ℃: (a) Dark field image, and (b) EDS of particle.

Table Captions:

Table 1 Chemical compositions of the studied steel (wt.%).

Table 2 RT Charpy impact results before and after heat treatment.

Table 3 Tensile properties of the furnace-cooled specimens.

Table 4 Results of composition analysis of precipitates obtained from spectra.

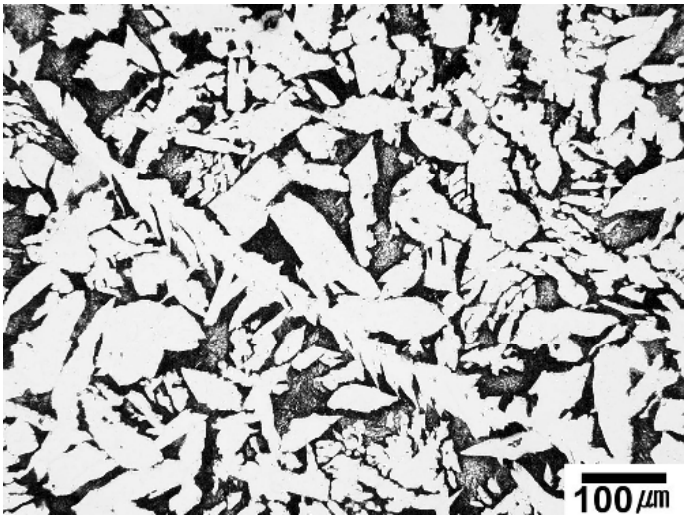

Fig. 1. Metallograph of the as-cast steel.

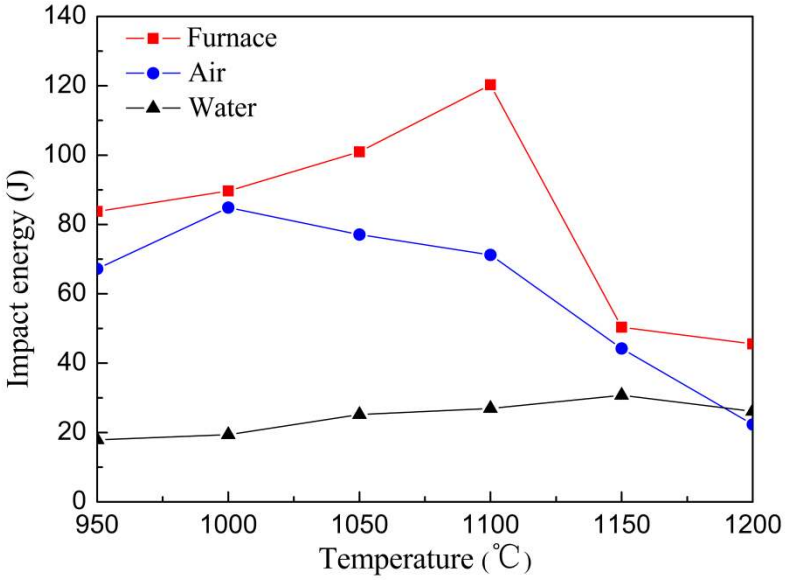

Fig. 2. Plots of RT impact energy vs. heat treatment temperature at various cooling conditions after 2 h austenitization.

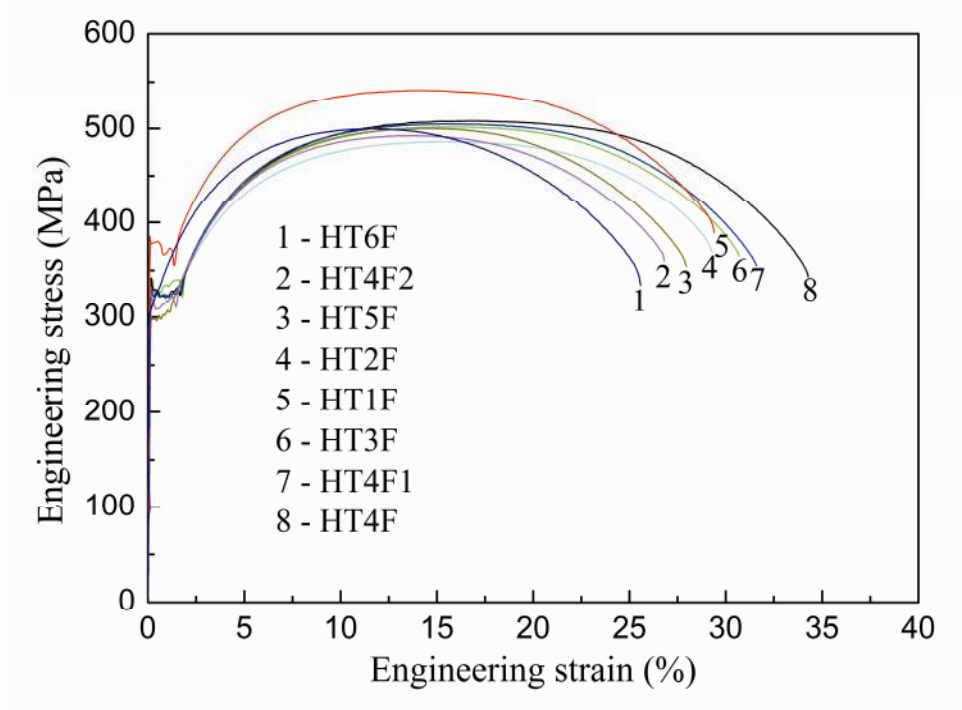

Fig. 3. Typical tensile curves of the furnace-cooled specimens.

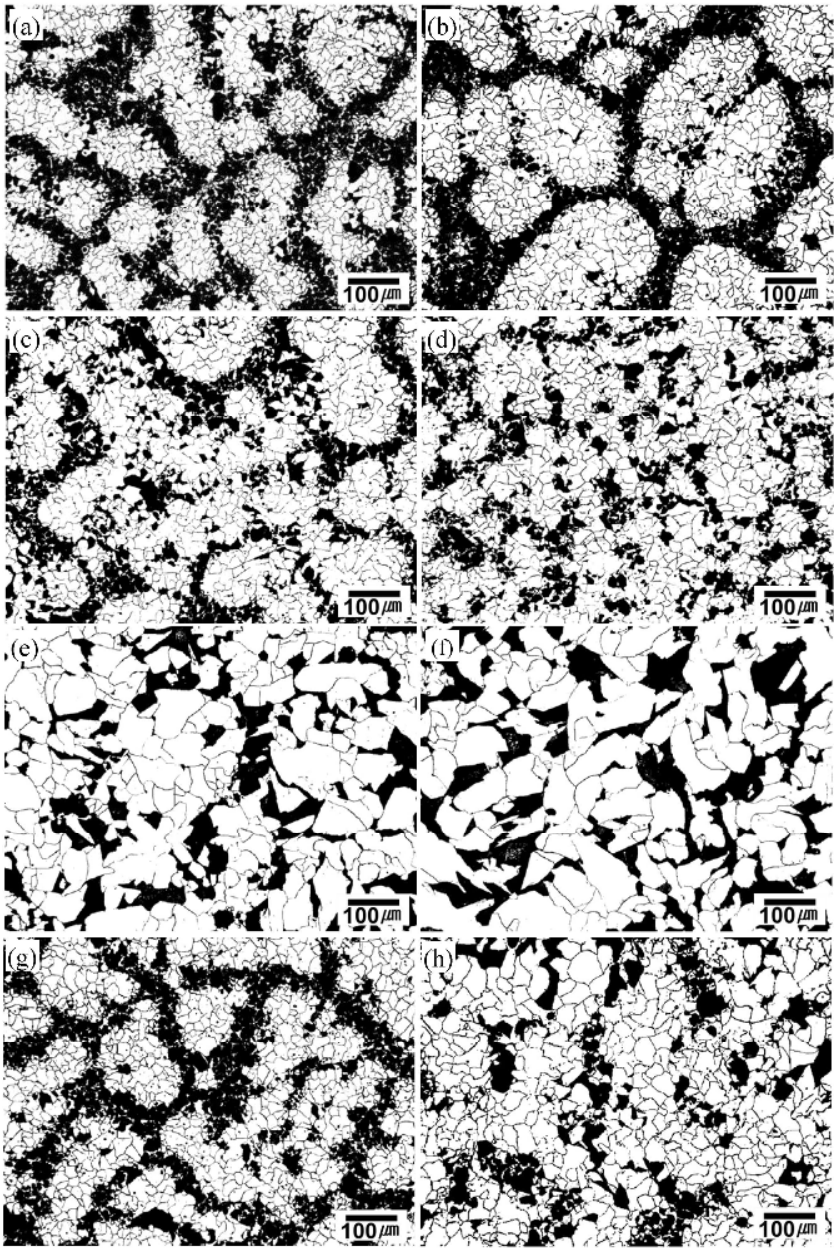

Fig. 4. OM microstructures of furnace-cooled specimens according to Table 2: (a) HT1F, (b) HT2F, (c) HT3F, (d) HT4F, (e) HT5F, (f) HT6F, (g) HT4F1, and (h) HT4F2.

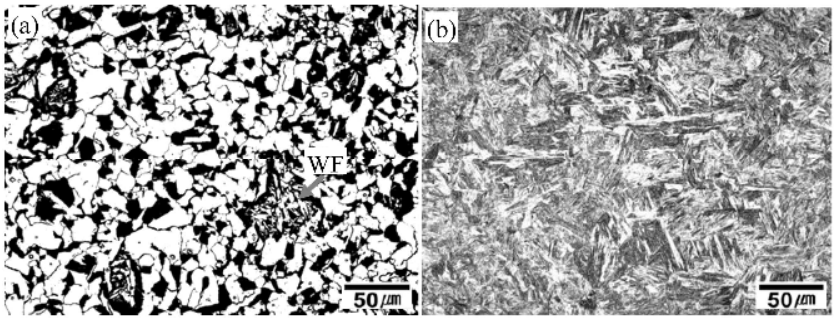

Fig. 5. OM microstructures of selected specimens according to Table 2: (a) HT4A, and (b) HT4W (etched by nital).

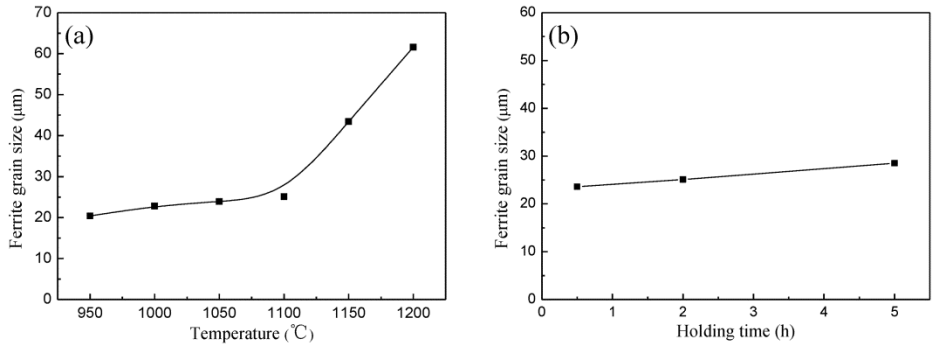

Fig. 6. Effect of temperature and holding time on ferrite grain size of the heat treated specimens after furnace cooling with (a) holding time of 2 h and (b) austenitizing temperature of 1100 ℃.

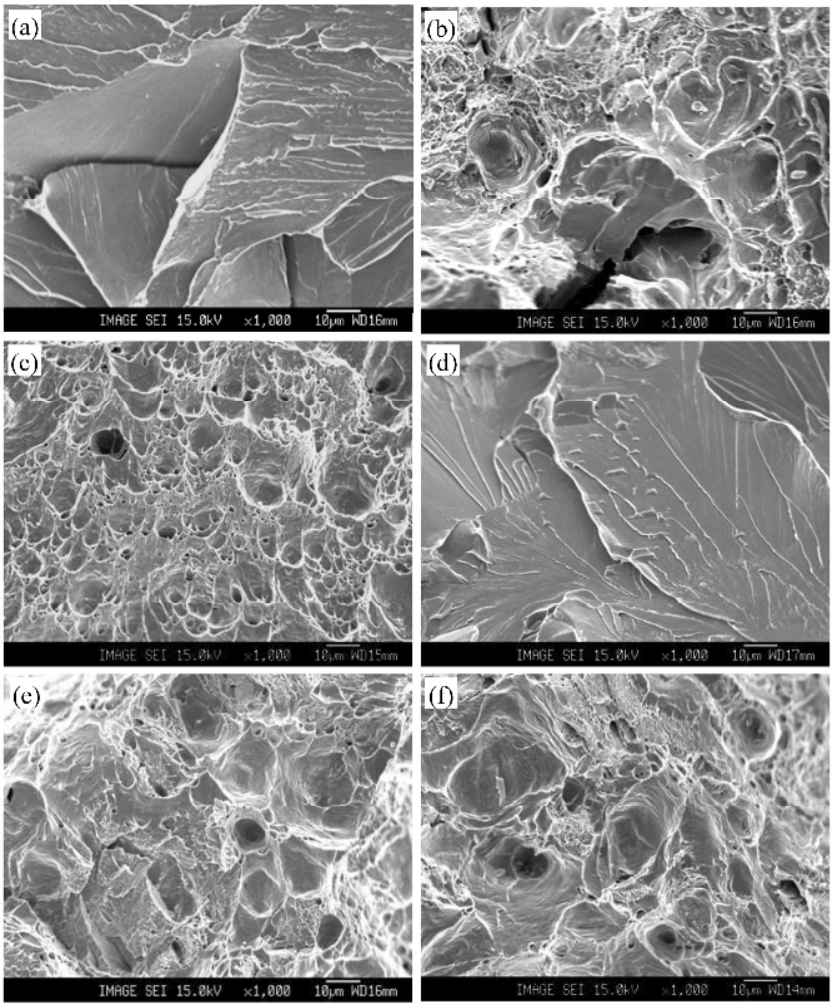

Fig. 7. Selected fracture surfaces in the shear lip areas of some impact test specimens according to Table 2: (a) HT0, (b) HT1F, (c) HT4F, (d) HT5F, (e) HT4F1, and (f) HT4F2.

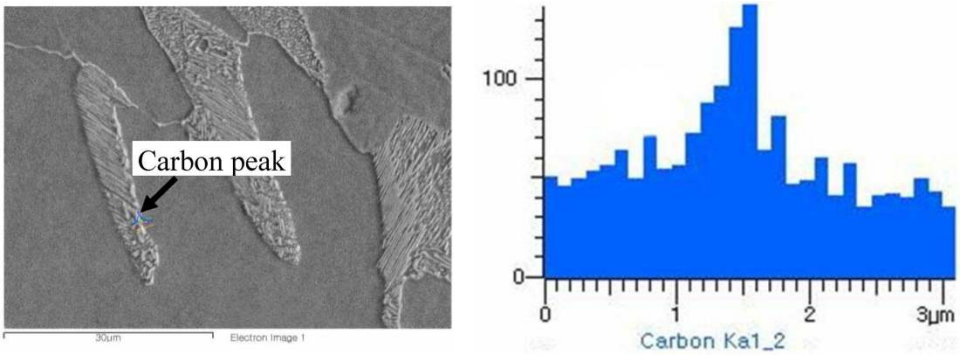

Fig. 8. Line-scanning for the as-cast specimen shows C segregation along dendrite boundary.

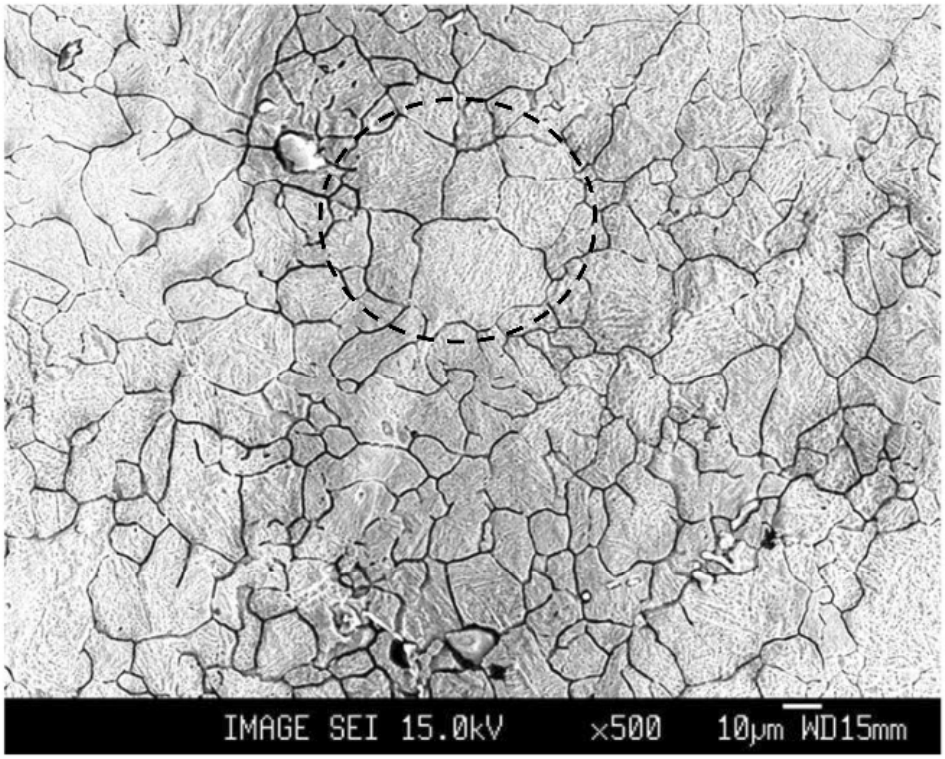

Fig. 9. SEM image of specimen HT1W shows non-uniform distribution of prior austenite grains.

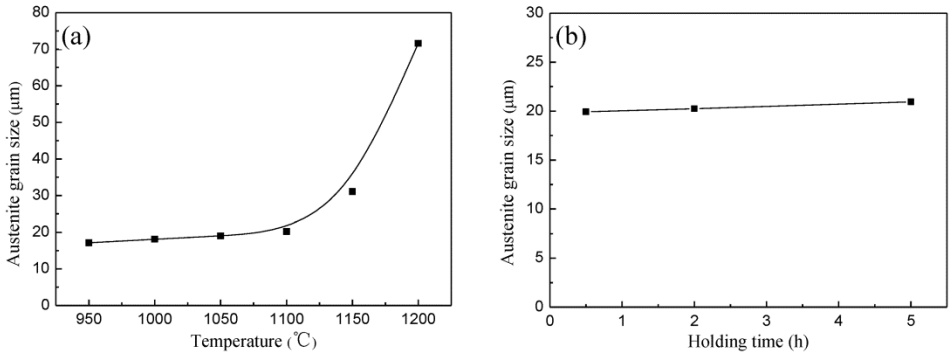

Fig. 10. Effect of temperature and holding time on the prior austenite grain size of the heat treated specimens after water quenching with (a) holding time of 2 h and (b) austenitizing temperature of 1100 ℃.

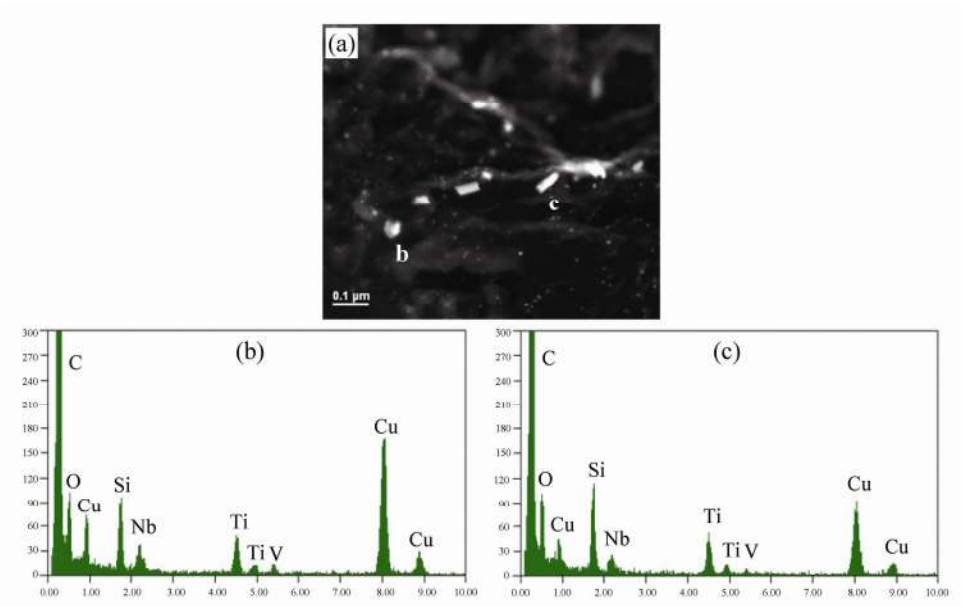

Fig. 11. Character and composition of precipitates in the specimen austenitized at 950 ℃: (a) Dark field image, (b) EDS of particle “b”, and (c) EDS of particle “c”.

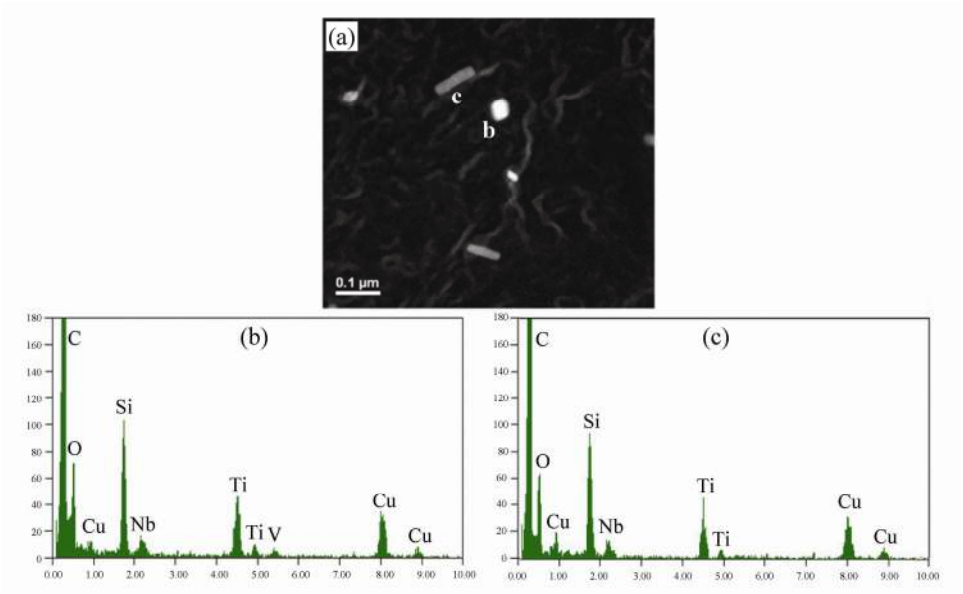

Fig. 12. Character and composition of precipitates in the specimen austenitized at 1100 ℃: (a) Dark field image, (b) EDS of particle “b”, and (c) EDS of particle “c”.

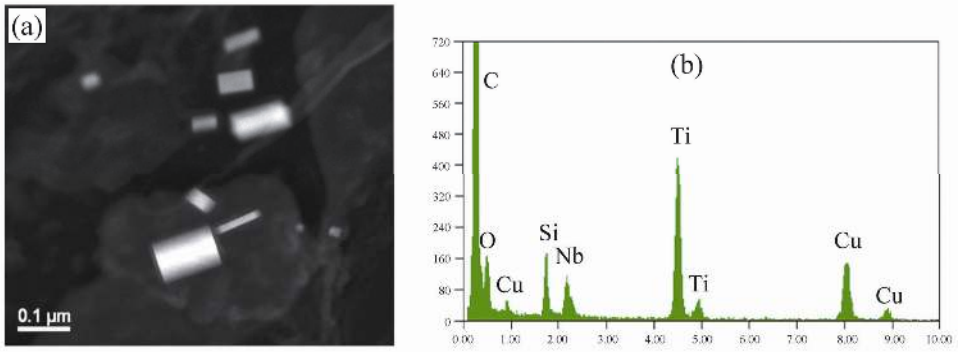

Fig. 13. Character and composition of precipitates in the specimen austenitized at 1150 ℃: (a) Dark field image, and (b) EDS of particle.

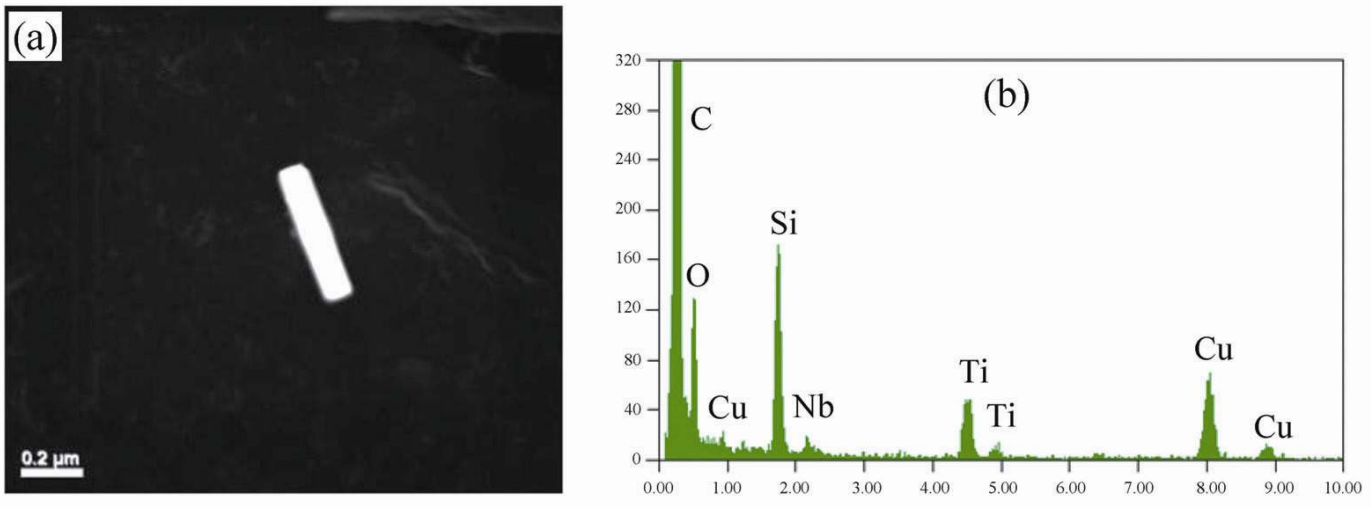

Fig. 14. Character and composition of precipitates in the specimen austenitized at 1200 ℃: (a) Dark field image, and (b) EDS of particle.

Table 1 Chemical compositions of the studied steel (wt.%).

C	Mn	Cr	Ni	Cu	Si	Al	V	Nb	Ti	P	S	N
0.17	1.2	0.1	0.02	0.02	0.47	0.02	0.01	0.02	0.02	0.01	0.01	0.006

Table 2 RT Charpy impact results before and after heat treatment.

Specimen	Austenitizing temperature (℃)	Holding time (h)	Cooling method	RT Impact energy (J)
HT0	As-cast	-	-	5.4
HT1F	950	2	Furnace	83.8
HT1A	950	2	Air	67.2
HT1W	950	2	Water	17.9
HT2F	1000	2	Furnace	89.7
HT2A	1000	2	Air	84.9
HT2W	1000	2	Water	19.4
HT3F	1050	2	Furnace	101.0
HT3A	1050	2	Air	77.1
HT3W	1050	2	Water	25.2
HT4F1	1100	0.5	Furnace	97.9
HT4F	1100	2	Furnace	120.3
HT4A	1100	2	Air	71.2
HT4W	1100	2	Water	27.0
HT4F2	1100	5	Furnace	111.0
HT5F	1150	2	Furnace	50.4
HT5A	1150	2	Air	44.2
HT5W	1150	2	Water	30.7
HT6F	1200	2	Furnace	45.6
HT6A	1200	2	Air	22.3
HT6W	1200	2	Water	26.2

Table 3 Tensile properties of the furnace-cooled specimens.

Specimens	YS (MPa)	UTS (MPa)	Elongation (%)
HT1F	378.5	541.6	29.4
HT2F	328.8	486.2	29.4
HT3F	341.1	501.9	30.8
HT4F1	335.4	505.1	31.6
HT4F	344.9	511.3	34.3
HT4F2	322.1	492.5	26.9
HT5F	299.2	500.1	27.9
HT6F	310.2	499.8	25.6

Table 4 - Results of composition analysis of precipitates obtained from spectra.

Temperature (℃)	Precipitates	Composition ratio (at.%)
950	Irregularly shaped	Ti:Nb:V=1:0.91:0.12
950	Rectangular	Ti:Nb:V=1:0.42:0.02
1100	Square	Ti:Nb:V=1:0.32:0.02
1100	Rectangular	Ti:Nb=1:0.29
1150	Rectangular	Ti:Nb=1:0.28
1200	Rectangular	Ti:Nb=1:0.43